Structural and Multidisciplinary Optimization (2022) 65:70
https://doi.org/10.1007/s00158-022-03175-3

RESEARCH PAPER

Inverse design of planar morphing scissor structures with end constraints

Qian Zhang[1,2] · Wenwen Jia[3] · Daniel Sang-hoon Lee[4] · Jianguo Cai[1] · Jian Feng[1]

Received: 18 June 2021 / Revised: 5 January 2022 / Accepted: 11 January 2022 / Published online: 31 January 2022

Abstract

Scissor structures can meet different performance goals by actively changing their geometric configurations. This paper focuses on the inverse design problem of planar scissor structures with end constraints to obtain various forms without changing the span. Two strategies are proposed, one based on adding hinges and the other based on telescopic rods. The corresponding geometrical principles and constraint conditions are formulated. An inverse design framework from two predefined target shapes to design parameters is established, which consist of geometry optimization and mobility assessment. Seven case studies are used to illustrate the design method based on the two strategies. Results show potential for application of morphing planar scissor structure in practice.

Keywords Inverse design · Morphing planar scissor structures · End constraints · Additional hinges · Telescopic rods

List of symbols

φ	Relative angle between straight beams in the rigid arm
A	Rigid arm
b^l, b^r	Lengths of left and right straight beams in the rigid arm
DOF	Degree of freedom
e, d	Constraint coordinates of the right-most node
F	Optimization result, also called configuration error
f_{P1}, f_{P2}	Two target shape functions
j_k	Node number of k-th hinge nodes
l	Length of straight beam for isometric arms
m	Number of hinge nodes
n	Number of scissor units
o	Internal connection node between the straight beams in the scissor unit
p^l, p^r	Left and right end nodes of rigid arms
P_1, P_2	Two target shapes in the optimization
$Q(X_j)$	Geometry parameter set of the j-th scissor unit
t	Configuration parameter, $1 \le t \le 2$
X	Scissor unit
$x_{o_j^1}^{P_t}, y_{o_j^1}^{P_t}$	Coordinates of the node o_j^1 at the target configuration P_t

1 Introduction

Morphing structures can achieve a wide range of performance goals by changing their geometric configuration (Li and Pellegrino 2020; Sachse and Bischoff 2021; Fenci and Currie 2017; Weaver-Rosen et al. 2020; Meloni et al. 2021). Geometry changes enable structures to perform optimally in multiple configurations, improving efficiency throughout their operating envelope. Compared to conventional mechanisms, morphing structures can offer many attractive properties. Morphing aircraft design can lead to a multi-purpose aerial vehicle by shape changes (Rhodes 2013; Sleesongsom et al. 2013). The shape adaptation can be employed as a design and control strategy to reduce material input and embodies energy for load-bearing structures (Wang and

Responsible Editor: Seonho Cho

✉ Jianguo Cai
j.cai@seu.edu.cn

[1] Key Laboratory of C & PC Structures of Ministry of Education, National Prestress Engineering Research Center, Southeast University, Nanjing 211189, China

[2] Department of Structural Engineering and Building Materials, Faculty of Engineering and Architecture, Ghent University, Valentin Vaerwyckweg 1, 9000 Ghent, Belgium

[3] Beijing Institute of Spacecraft System Engineering, Beijing 100094, China

[4] School of Architecture, Design and Conservation, Institute of Architecture and Technology, The Royal Danish Academy of Fine Arts, Copenhagen 1435, Denmark

Senatore 2020, 2021; Senatore and Reksowardojo 2020). The transformable scissor structure is an effective way to design morphing structures (Arnouts et al. 2020; Yang et al. 2019; Kim et al. 2021; Zhang et al. 2021). A transformable Cable Scissors Arch (CSA) has been proposed to achieve a continuous geometry change of the roof structure from a plane to a cylinder, where the flexible zigzag cables were used between the scissors units (Kokawa and Hokkaido 1997). Extendable members were introduced to design a flexible truss called Variable Geometry Truss (VGT) (Inoue et al. 2006). Variable truss shapes were obtained by controlling the lengths of extendable members, and the method was used to design a movable sculpture for EXPO 2005 in Japan. Moreover, shape morphing can be employed to effectively counteract the effect of loading, resulting in significant material and energy input savings. Reksowardojo et al. (2019, 2020). The adaptive design was also investigated for the slender high-rise structures, arch bridges (Senatore and Reksowardojo 2020) and tested experimentally on a nearly full scale prototype structure (Senatore et al. 2017).

Morphing scissor structures can be classified as foldable and incompatible structures based on the folding behavior (Arnouts et al. 2019). Foldable scissor structures behave like mechanisms during the transformation process. No stress is caused during shape adaptation. However, shape control relies on external actuation. On the contrary, incompatible scissor structures are geometrically incompatible throughout the transformation process (Arnouts et al. 2020; Kawaguchi et al. 2019), and thus stress is induced during shape adaptation. This paper focuses on the morphological transformation requirements of foldable scissor structures. For temporary structures that require fast construction, foldable scissors could have many applications. Emergency bridges based on the scissor structures have been proposed to recover after the occurrence of natural disasters (Ario et al. 2013; Chikahiro et al. 2016). To provide different traffic modes for ships or pedestrians, the scissor mechanism was introduced in the design of a footbridge in Geneva. Different shape configurations have been achieved through active control of hydraulic cylinders installed at the supports (Bouleau and Guscetti 2016). Scissor-type evacuation shelters have been investigated for greater mobility and reusability (Alegria Mira et al. 2014; Lee et al. 2013). A deployable and reconfigurable planar structure, consisting of serially connected rigid members and actuators, was proposed by Phocas et al. (2015, 2020). Scissor-like structures have also been used to design a novel vibration isolation platform (Sun and Jing 2016), lift mechanisms (Zhao et al. 2016) and space antennas (Han et al. 2019).

There are three distinct basic unit types that are often used to design morphing scissor structures: translational, polar and angulated units. Structures made from these components have only one degree of freedom, and therefore shape control is limited (Gantes 1991). Modified scissor components have been proposed to increase shape morphing capability. Hinges are added in the linear array of polar scissor units to form the supporting structure of an origami membrane surface (Van Mele 2008). Modified scissor units were designed by releasing the relative rotation angle constraints between the straight beams in one rigid arm (Akgün et al. 2010, 2011). Then, novel transformation models for deployable planar and spatial scissor structures were developed, which allowed the structure to switch between rectilinear geometries and double-curved forms. Telescopic rods were introduced to deal with the incompatibility of bistable scissor structures and increase design flexibility (Lim et al. 2014).

For the design of morphing scissor structures, the deductive approach has been investigated by choosing basic typology types of scissor units and by deriving geometric principles and design rules. However, this method is only suitable for simple design and requirements. Zhao et al. (2009) proposed a formulation to investigate the application of different scissor units for flat, cylindrical and spherical deployable structures. The formulation has also been applied to analyze the kinematic behavior of Hoberman's linkages (Cai et al. 2013). Maden et al. (2011) developed methods for different types of scissor structural mechanisms. General principles that govern the motion and shape of scissor grids consisting of translational units have been given by Roovers and De Temmerman (2017). A geometric design method for axisymmetric grid structures made of three-dimensional angulated scissor units on a regular polygonal base was presented by Krishnan and Liao (2020). A new geometric method was also proposed to design bistable and non-bistable deployable structures using straight scissors (García-Mora and Sánchez-Sánchez 2020), which has been further developed into the convergence surface method (García-Mora and Sánchez-Sánchez 2021). A deductive approach is not suitable for analyzing complex morphing structures, hence inductive approaches have also been investigated. Alegria Mira et al. (2015) established a two-steps evaluation framework that includes parametric analysis to study the influence of height, span, number of units and scissor type on the structural behavior (e.g., stress, deflection and required material mass). This design method requires a large number of example analysis, and the relationship between design parameters and configuration parameters should be obtained by comparison and induction.

Optimization methods have also been investigated to design scissor structures. Two different multi-objective algorithms NSGAII and MOCBO were utilized effectively by Kaveh and Abedi (2019) for the optimum design of foldable structures that results in minimum weight and volume. The reinforcement layout for bridges, consisting of scissor structures, was evaluated by Chikahiro et al. (2019) using a

combination of finite element analysis and an optimization algorithm to reduce the weight and increase the stiffness. An inverse design method was also proposed to design planar deployable structures made of scissor structure components (Zhang et al. 2015). A feasible motion solution was obtained to move from the initial shape to the target shape. However, deflections and stresses are not constrained during the development. Moreover, the method has not been extended to morphing scissor structures with end constraints, which can be applied in several scenarios, such as arch bridges with variable heights.

This paper focuses on the inverse design problem of planar scissor structures with end constraints. To overcome the incompatibility during the transformation between two predefined target configurations, we propose two strategies to increase the design flexibility by adding hinges and telescopic rods in the scissor unit. After topology determination, an inverse design framework is established, consisting of geometry optimization and mobility assessment, which is illustrated through seven case studies.

2 Planar scissor structures with additional hinges

2.1 Problem description

The proposed planar scissor structures are composed of coplanar scissor units. The basic geometrical description of a unit is given in Fig. 1a. It consists of two rigid arms $A = \{p^l, o, p^r\}$, that can rotate around a hinge connection. Two straight beams compose one rigid arm, with lengths b^l (left straight beam), b^r (right straight beam) and a constant relative angle φ between the two straight beams. The scissor unit is denoted as $X = \{A^1, A^2\} = \{p^{1,l}, o^1, p^{1,r}; p^{2,l}, o^2, p^{2,r}\}$, and we call $o^1 = o^2$ the revolute joint, $\{p^{1,l}, p^{1,r}, p^{2,l}, p^{2,r}\}$ the pin nodes. Noticeably, there is only one motion degree of freedom (DOF) for the scissor unit due to the revolute joint.

For example, a planar arch scissor structure is designed with end constraints, as shown in Fig. 1b. The scissor arch structure has no motion DOF because of the end constraints. It cannot move to the target configurations P_1 and P_2 freely because there is no feasible movement path. To achieve the design of morphing planar scissor structures, additional hinges are introduced to replace the revolute joint to increase the number of DOFs. In the hinge joint, the constraints on the relative angle between the straight beams are removed compared to the revolute joint. This way, an inverse design problem emerges to obtain geometry parameters of an arch scissor structure that can be controlled into the required target configurations. Before the inverse design, we should determine the topology first. The topology consists of the number of scissor units n, number of hinged nodes m, and the initial arrangement of nodes. The geometry parameters are the lengths of straight beams and the coordinates of hinge nodes.

In this article, the requirement of only two target configurations is discussed. Such a design task is challenging. No established and general design methodology exists to solve such a problem. Trial and intuitive solutions are not applicable when dealing with complex scissor systems. In addition, the definition of mechanical and motion constraints is required and must be validated.

2.2 Design method of planar scissor structures

Based on the given two-dimensional target curves, the topology design is carried out to obtain the basic configuration of the plane scissor mechanism before optimization. The number

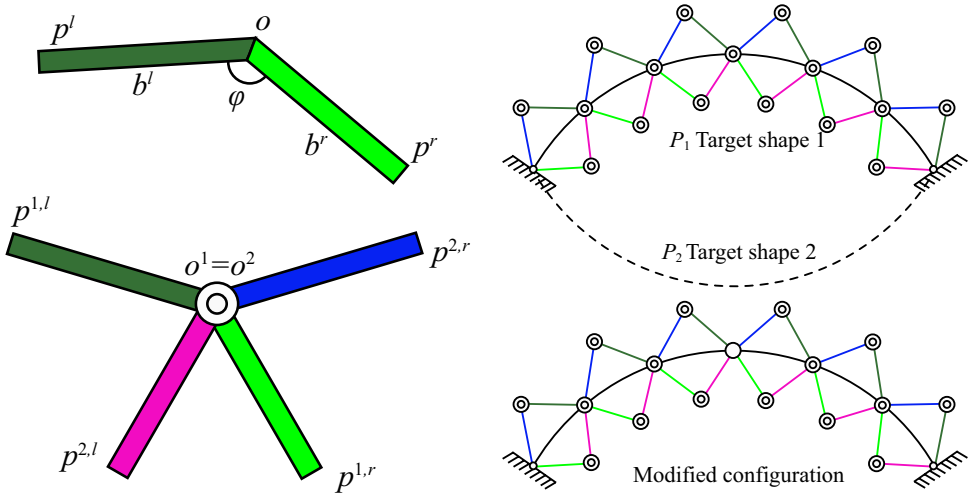

(a) Notation of a scissor unit **(b)** Modified configuration design

Fig. 1 Design schematic of a planar arch with scissor components and hinges

of scissor units n, the number of hinge nodes m, and the assemblage of the scissor system are given. The number of degrees of freedom (DOFs) of the mechanism is then determined. The boundary constraint conditions of the morphing scissor structures are determined. Then, the design of morphing scissor structures can be decomposed into two main steps: geometry optimization and motion assessment. The detailed inverse design and analysis procedure can be described as follow.

Step(a) *Geometry optimization* (1) The values of the geometric parameters of the scissor structures are initially given before the start of the optimization. (2) The geometrical parameters of the system are optimized to control the structure into the target configurations P_1 and P_2 with a given error. (3) The geometric parameters include the length of straight beams and the coordinate values of each hinged node so that the structures can further approach the targeted curves. (4) If the error is large, a new topology must be defined.

Step(b) *Motion assessment* After obtaining a planar scissor structure that can morph into the two target shape configurations, intermediate stages are obtained to optimize the coordinates of the hinge nodes. This process is employed to verify the motion feasibility across the controlled configurations, which includes assessing whether the motion path can be realized stress-free under the preassigned end constraints.

Step(a). The design of a scissor structure with two target shapes is defined as a constrained optimization problem. Geometrical definitions of the curves (P_1, P_2) and the topological parameters (n, m) are given. The geometric parameters, $Q\left(X_j\right)_{j=1}^{n}$ of the scissor and the coordinates of the hinge nodes are the optimization variables. All relative angles of the straight beams in the scissor units are assumed to be the same.

$$\begin{aligned} &Q(X_j)_{j=1}^{n} = \left\{ b_j^{1,l}, \varphi_j^1, b_j^{1,r}, b_j^{2,l}, \varphi_j^2, b_j^{2,r} \right\}; \\ &\left\{ \left(x_{o_{jk}}^{P_1}, y_{o_{jk}}^{P_1} \right), \left(x_{o_{jk}}^{P_2}, y_{o_{jk}}^{P_2} \right), 1 \le j_k \le n \right\}_{k=1}^{m}. \end{aligned} \tag{1}$$

where $\{(x_{o_{jk}}^{P_1}, y_{o_{jk}}^{P_1}), (x_{o_{jk}}^{P_2}, y_{o_{jk}}^{P_2})\}$ are the coordinates of the k-th hinge node in the target shapes P_1 and P_2, respectively. For clarity, the coordinates of the hinge nodes are different for the two target shapes, while the topology remain unchanged. The objective function is defined as the minimization of the position deviations of hinge nodes and revolute joint with respect to the target curves.

$$F = min \sum_{j=2}^{n-1} \left\{ \left[f_{P_1}\left(x_{o_j}^{P_1} \right) - y_{o_j}^{P_1} \right]^2 + \left[f_{P_2}\left(x_{o_j}^{P_2} \right) - y_{o_j}^{P_2} \right]^2 \right\}. \tag{2}$$

where F is the optimization results, also called configuration error, f_{P_1} and f_{P_2} are the functions for two target curves. In the absence of a common reference shape, the similarity between controlled and target shapes should not be evaluated based on Euclidean distance because it cannot be normalized. Shape similarity could be assessed rigorously using a metric that accounts of the similarity of node coordinates as well as shape features and that can be normalized across multiple target shapes as formulated in ref Reksowardojo et al. (2020). However, for simplicity and because a maximum of two target shapes is considered, the configuration error is computed based on the Euclidean distance between the node coordinates of controlled and target shapes. At different configuration parameter t, the constraint conditions are length constraints for the straight beams, relative position constraints for all nodes, relative rotation constraints between the straight beams and boundary constraints.

Length constraints for the straight beams at $t = 1, 2$:

$$\begin{aligned} &(x_{o_j^1}^{P_t} - x_{p_j^{1,r}}^{P_t})^2 + (y_{o_j^1}^{P_t} - y_{p_j^{1,r}}^{P_t})^2 = l^2, (x_{o_j^2}^{P_t} - x_{p_j^{2,r}}^{P_t})^2 + (y_{o_j^2}^{P_t} - y_{p_j^{2,r}}^{P_t})^2 = l^2, 1 \le j \le n-1; \\ &(x_{o_j^1}^{P_t} - x_{p_j^{1,l}}^{P_t})^2 + (y_{o_j^1}^{P_t} - y_{p_j^{1,l}}^{P_t})^2 = l^2, (x_{o_j^2}^{P_t} - x_{p_j^{2,l}}^{P_t})^2 + (y_{o_j^2}^{P_t} - y_{p_j^{2,l}}^{P_t})^2 = l^2, 2 \le j \le n. \end{aligned} \tag{3}$$

Relative position constraints for all nodes at $t = 1, 2$:

$$\begin{aligned} &o_j^{1,P_t} = o_j^{2,P_t}, 1 \le j \le n; \\ &p_j^{2,r,P_t} = p_{j+1}^{1,l,P_t}, p_j^{1,r,P_t} = p_{j+1}^{2,l,P_t}, 1 \le j \le n-1. \end{aligned} \tag{4}$$

Relative rotation constraints between the straight beams in the rigid arms at $t = 1, 2$:

$$\begin{aligned} &\mathrm{X}_{p_j^{1,l} o_j^1}^{P_t} \times \mathrm{X}_{o_j^1 p_j^{1,r}}^{P_t} - l^2 \sin\varphi = 0; \\ &\mathrm{X}_{p_j^{2,l} o_j^2}^{P_t} \times \mathrm{X}_{o_j^2 p_j^{2,r}}^{P_t} - l^2 \sin\varphi = 0. \end{aligned} \tag{5}$$

Boundary constraints for the two end nodes:

$$x_{o_1^1} = y_{o_1^1} = 0, x_{o_n^1} = e, y_{o_n^1} = d. \tag{6}$$

The designed scissor system must satisfy the transformation requirement from the first target shape P_1 to the second target shape P_2. The problem has been formulated as a non-linear programming problem that has been solved using interior-point algorithm built-in Matlab. There are continuous optimization variables in a closed convex set. The convexity of optimization problem will depend on the convexity of objective functions, which are related to the target curves. If there is a non-convex objective function, the optimization problem must be non-convex. Optimization will complete when the objective function is non-decreasing in feasible directions or within the optimal tolerance value.

Step(b). The feasible movement paths are investigated between the two controlled shapes, that might be different

from the prescribed target shapes depending on the error. There may be an infinite number of movement paths to move across the two target shapes. In this work, it is assumed a sequential linear interpolation between the target shapes through intermediate stages. For an assumed motion time t, the target coordinates of the hinge nodes and revolute joints can be expressed through interpolation for $1 \le t \le 2$, and $1 \le j_k \le m$.

$$\begin{aligned} x_{o_{j_k}}^{P_t} &= x_{o_{j_k}}^{P_1} + (t-1)\left(x_{o_{j_k}}^{P_2} - x_{o_{j_k}}^{P_1}\right); \\ y_{o_{j_k}}^{P_t} &= y_{o_{j_k}}^{P_1} + (t-1)\left(y_{o_{j_k}}^{P_2} - y_{o_{j_k}}^{P_1}\right). \end{aligned} \tag{7}$$

In step (b) (motion assessment), only the coordinates of the additional hinge nodes are regarded as the optimization variables. There is no change in the geometry parameters and other constraint conditions. Then, the motion condition can be described as the existence of feasible solutions for coordinates of the additional hinge nodes. An arbitrary intermediate state can be expressed through interpolation. If the intermediate states can not be achieved, a lock occurs during the movement path. In this manuscript, five intermediate states are considered.

The actuation design depends on the analysis of degrees of freedom. The relative rotations of rigid arms can be chosen as the actuation control parameters. Besides, the relative distances between the pin end nodes on each of the sides of the scissor units can be chosen to control the motion, such as the distance between $p^{1,l}$ and $p^{2,l}$.

2.3 Case studies for scissor components with additional hinges

2.3.1 Case 1

In this case, two symmetrical sine curves are taken as the target shapes, given by $f_{P_1} = 500\sin(\pi x/3000)$ and $f_{P_2} = -500\sin(\pi x/3000)$, respectively. In the step of topology determination, the morphing planar scissor structure is predesigned with five scissor units and one additional hinge node, as shown in Fig. 2a. Note that four straight beams can rotate by each other about the additional hinge node o_3. The other nodes are revolute joints that allow the rigid arms can rotate by each other. The lengths of the straight beams and the relative angles for all scissor elements are the same, represented by l and φ, respectively. The initial values are given in Table 1.

Figure 2b illustrates the two optimized configurations. The final geometric parameters and the coordinate values of the additional hinge node o_3 are given in Table 1. Note that the relative angles between the straight beams in the rigid arms would need to be 180°, in this configuration which means that the scissor units degenerate into parallel units. There is a deviation between the target and controlled shapes.

Table 1 Geometry optimization results for Case 1

States	l (mm)	φ(°)	x_{o_3}	y_{o_3}	Configuration error (mm^2)
Initial	619.86	161.32	1500	955	2.06e+06
Curve P_1	516.04	180.00	1500	569	2.86e+04
Curve P_2			1500	− 569	

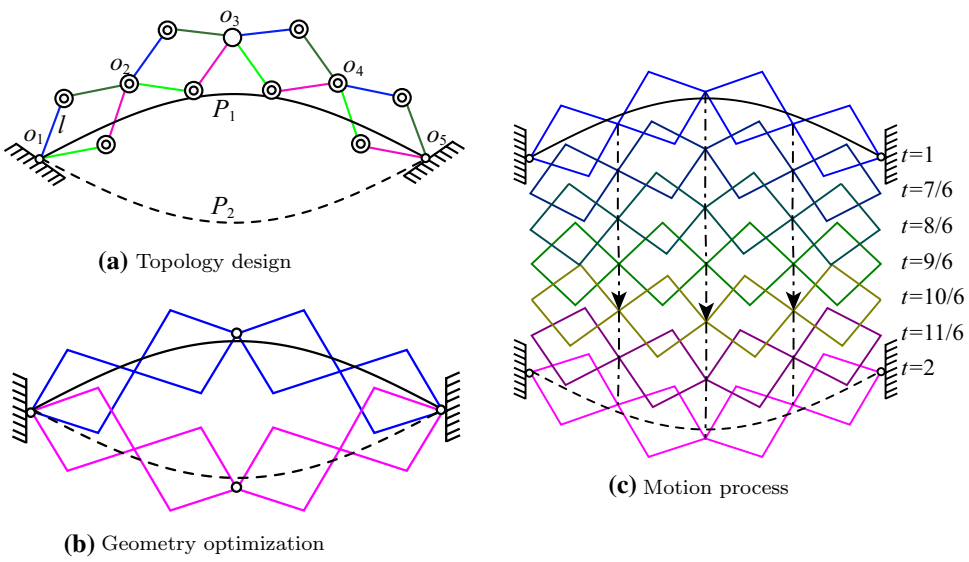

(a) Topology design

(b) Geometry optimization

(c) Motion process

Fig. 2 Case 1, one additional hinge and isometric arms

The average coordinate error with respect to the length of the straight beam, which is defined as $\sqrt{F/2(n-2)}/l$, is 13.4%. For accurate shape control the average coordinate error should smaller than 1%, therefore it can be concluded that the planar scissor structure can not be transformed into the target shapes by adding only one middle hinge.

Verification of motion is performed at five different steps, $t = 7/6, 8/6, 9/6, 10/6, 11/6$, which are equally spaced within the initially given time frame, $1 \le t \le 2$. Table 2 shows that the morphing scissor structure can transform between the two optimized configurations without locking based on the current parametric conditions, although there are significant deviations between the optimized and predesigned target shapes. It should be clarified that the configuration errors are calculated between the optimized and predesigned target shapes, while the motion assessment is performed between the two obtained controlled configurations, independent of the prescribed target configurations. Figure 2c illustrates the intermediate configuration of the planar scissor structure during the motion. Table 2 gives the errors between the intermediate shapes and intermediate target curves obtained through linear interpolation. If the error is smaller than 1e−6, there is a stress-free motion path between the controlled shapes.

Table 2 Motion analysis for Case 1

States	$x_{o_3}^{P_t}$	$y_{o_3}^{P_t}$	Optimization results (mm^2)
$t = 7/6$	1500	379	8.85e−07
$t = 8/6$	1500	190	2.28e−07
$t = 9/6$	1500	0	1.96e−07
$t = 10/6$	1500	− 190	2.28e−07
$t = 11/6$	1500	− 379	8.85e−07

2.3.2 Case 2

To obtain a better match of the target shapes, the length constraints are relaxed in this case. It is not necessary for all the straight beams to be equal in length, as shown in Fig. 3a. The straight beam lengths are denoted as l_1 to l_{16}, while the relative angles for all rigid arms remains the same. The topology design in Case 2 is the same as that in Case 1, and the optimization procedure is carried out again.

Figure 3b shows that the revolute joints (o_2 and o_4) and hinge nodes (o_3) of the optimized configurations are in good alignment with the two target curves. The coordinate errors are reduced from Case 1, as shown in Table 3. A feasible solution has been obtained owing to the increase of optimization variables. The distribution of the straight beam lengths is asymmetric. The maximum difference in beam length reaches 64.9% between l_1 and l_{12}. Moreover, the scissor structure can transform between the two target configurations without stress arising from the moving process, which is illustrated in Fig. 3c. The configuration error in the motion path is smaller than 1e−6, which shows the motion path is stress-free.

2.3.3 Case 3

The planar scissor structure in Case 3 is comparable to Case 1, except that all the intermediate nodes are hinge nodes, as shown in Fig. 4a. Topology and geometric constraints are the same as Case 1. The straight beams have identical lengths, and there are three additional hinge nodes (o_2, o_3, and o_4).

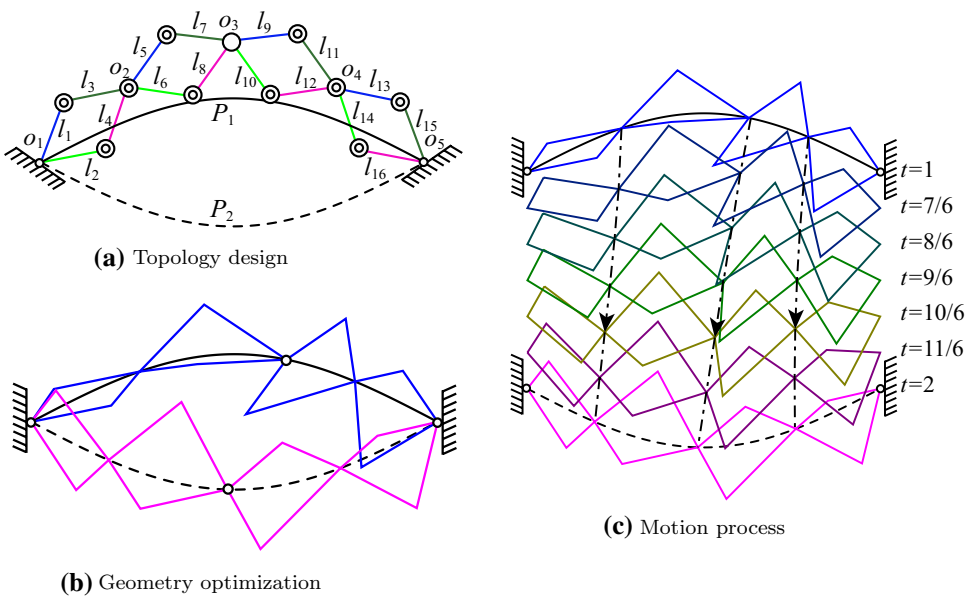

(a) Topology design

(b) Geometry optimization

(c) Motion process

Fig. 3 Case 2, one additional hinge and different length arms

The geometry optimization step and motion assessment step are carried out similarly.

Results in Table 4 and Fig. 4b show that the optimized scissor system can morph into the two target shapes with a small error. There is only 0.65% discrepancy between the optimized length of beams in Case 1 and Case 3. There are no rigid arms in the scissor structure. All relative angles between straight beams in rigid arms are no longer constant during motion. Moreover, relative angles for these units are different. The relative angle is no longer regarded as the control geometry parameter of structural design. The stress-free motion path of the optimized planar scissor structure between two controlled states is illustrated in Fig. 4c.

2.3.4 Case 4

In Case 4, the geometrical definitions of the two target curves are set as $f_{P_1} = 2000\sin(2\pi x/6000)$ and $f_{P_2} = 600\sin(\pi|x-3000|/3000)$. Since there is a significant difference between the two target shapes, the scissor structures with the increased number of scissor units is required to morph into the target geometries P_1 and P_2. The number of scissor units and hinge nodes are increased to $n = 9$ and $m = 3$, respectively. The beam lengths and the angles between the straight beams are all the same, respectively.

The configurations in Fig. 5 show that the scissor structure is divided into four parts with a symmetrical layout due to the

Table 3 Geometry optimization results for Case 2

States	Lengths of beams (mm)	$\varphi(^\circ)$	x_{o_3}	y_{o_3}	Configuration error (mm^2)
Initial	619.86	161.32	1500	955	2.06e+06
Curve P_1	$l_1 = 294.66$, $l_2 = 602.66$, $l_3 = 645.51$, $l_4 = 326.67$, $l_5 = 687.07$, $l_6 = 429.07$, $l_7 = 730.21$, $l_8 = 659.23$, $l_9 = 531.66$, $l_{10} = 501.96$, $l_{11} = 468.84$, $l_{12} = 840.25$,	175.86	1833	460	1.18e−10
Curve P_2	$l_{13} = 362.11$, $l_{14} = 635.33$, $l_{15} = 456.05$, $l_{16} = 654.94$		1450	− 499	

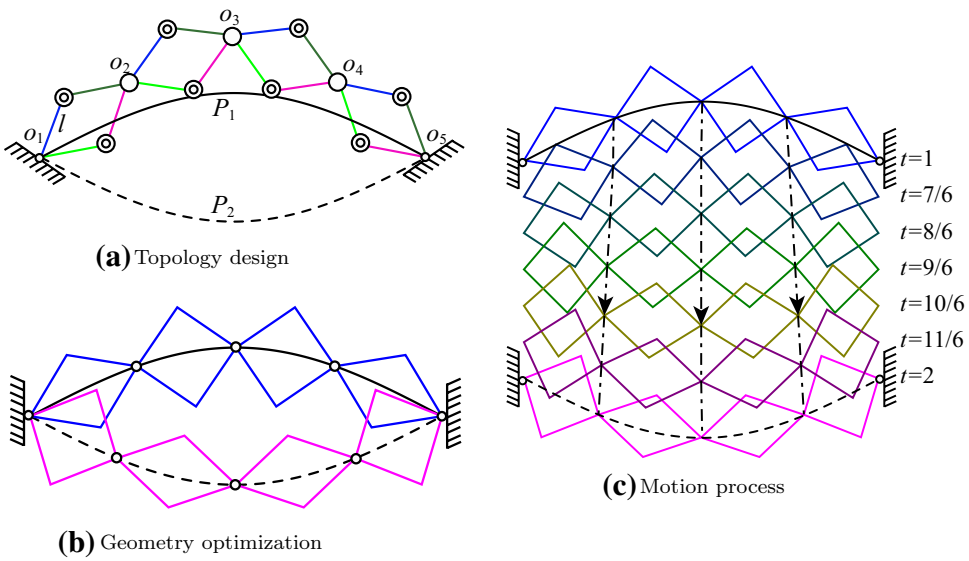

Fig. 4 Case 3, three additional hinge and isometric arms

Table 4 Geometry optimization results for Case 3

States	l	x_{o_2}	y_{o_2}	x_{o_3}	y_{o_3}	x_{o_4}	y_{o_4}	Configuration error (mm^2)
Initial	619.86	628	− 2325	144	− 1965	2259	− 2325	2.06e+06
Curve P_1	519.42	779	364	1500	500	2221	364	5.05e−11
Curve P_2		631	− 307	1500	− 500	2371	− 307	

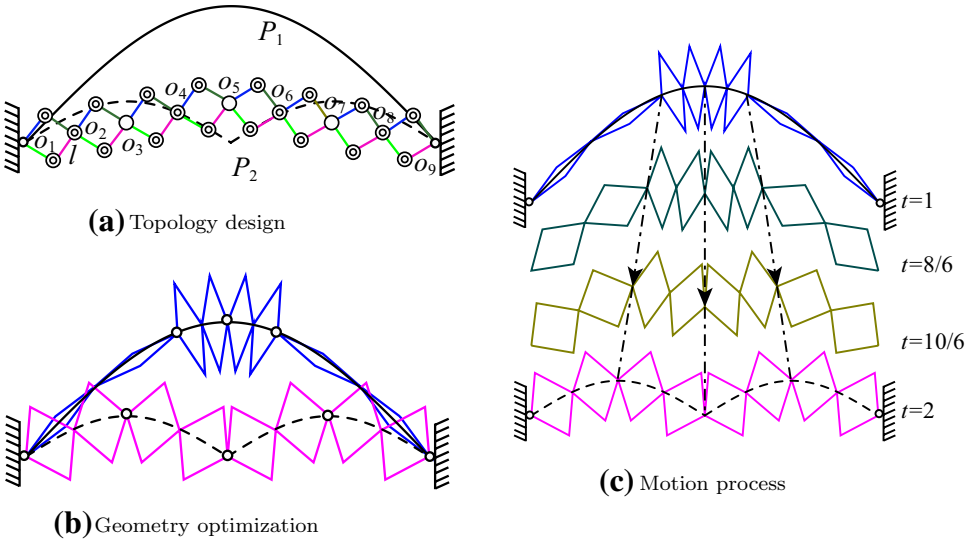

Fig. 5 Case 4, eight scissor units, three additional hinges and isometric arms

shape of the second target curve P_2. To morph into the target curve P_1, the two end parts approach the fully expanded state, while the two middle parts approach to the fully folded state. However, the four parts have the same configuration to morph into the second target shape P_2. Results in Table 5 show that the average coordinate error is 1.94% of the length of the straight beam, which is larger than the set limit. Figure 5c illustrates the stress-free motion process of the optimized planar scissor structures. The two end scissor components from both sides fold while the components in the middle unfold to morph between the two controlled configurations.

2.3.5 Case 5

The planar scissor system in Case 5 is identical to that of Case 4, except that the second target curve definition is changed to $f_{P_2} = 600\sin(2\pi x/6000)$. The left parts of shapes in these two cases are the same, while the right parts are mirrored. The optimization problems in Case 4 and Case 5 are non-convex. From the optimization results shown in Table 6 and Fig. 6b, it can be seen that the optimized length of the straight beams is larger than that in Case 4, and the average coordinate error reaches 5.06% of the length of the straight beam. Most of the intermediate nodes are close to the target curves, while there is a clear offset for node o_6 to target curve P_2. Compared with Case 4, Case 5 has more constraints, and the configuration error of Case 5 is larger than that of Case 4. Figure 6c illustrates the moving process from the symmetrical target shape P_1 to the antisymmetric target shape P_2. No lock occurs during motion, which indicates that there is a feasible linear stress-free motion path between the two target states.

3 Planar scissor structures equipped with telescopic rods

3.1 Scissor unit configuration with telescopic rods

Telescopic rods are introduced in the planar scissor structures to increase the morphing ability by increasing the number of degrees of freedom. Additional variable parameters are introduced to model the length variation of the straight beams in the rigid arms g. The length variation of the telescopic rod varies from 0 to f, The modified scissor unit, which is illustrated in Fig. 7, is denoted as $X^T = \{p^{1,l},s^{1,1},s^{1,2},o^1,s^{4,2},s^{4,1},p^{1,r};p^{2,l},s^{2,1},s^{2,2},o^2,s^{3,2},s^{3,1},p^{2,r}\}$. There are eight length parameters $\{g^1,b^{1,l},b^{1,r},g^3;g^2,b^{2,l},b^{2,r},g^4\}$. The corresponding maximum elongations of the telescopic rods are f^1, f^3, f^2, and f^4, respectively.

The inverse design process of scissor structures equipped with telescopic rods is similar to that of structures with additional hinges, except for the optimization variables. The hinge nodes coordinates are replaced by the lengths of the telescopic rods. In the topology determination step, the arrangement of the scissor units is set first. For the two controlled configurations and the

Table 5 Geometry optimization results in Case 4

States	l (mm)	$\varphi(^\circ)$	x_{o_3}	y_{o_3}	x_{o_5}	y_{o_5}	x_{o_7}	y_{o_7}	Configuration error (mm^2)
Initial	520.35	180.00	1500	300	3000	600	4500	300	9.90e+06
Curve P_1	739.15	167.43	2254	1837	3000	2000	3746	1837	2.89e+03
Curve P_2			1500	617	3000	0	4500	617	

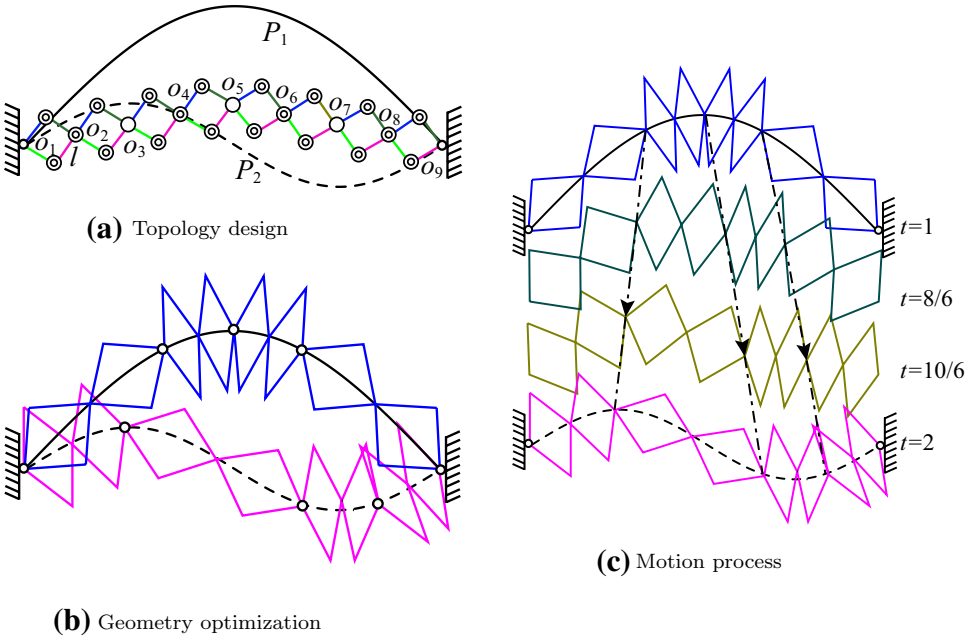

Fig. 6 Case 5, eight scissor units, three additional hinges and isometric arms

Table 6 Geometry optimization results in Case 5

States	l (mm)	φ(°)	x_{o_3}	y_{o_3}	x_{o_5}	y_{o_5}	x_{o_7}	y_{o_7}	Configuration error (mm^2)
Initial	520.35	180.00	1500	300	3000	600	4500	300	1.63e+13
Curve P_1	886.71	171.69	2019	1752	3027	2016	4013	1732	2.82e+04
Curve P_2			1471	613	4039	− 537	5143	− 504	

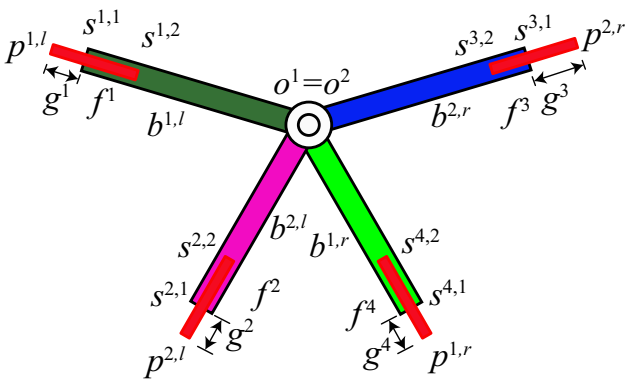

Fig. 7 A modified scissor unit with telescopic rods

motion process, the elongations of the telescopic rods are different. The analysis of two cases will be carried out to illustrate the inverse design method of the morphing planar scissor structures with end constraints equipped with telescopic rods. In addition to controlling the relative rotation angle of rigid arms and relative distance of end nodes on the same sides, changing the length of the telescopic rod can also realize the control of the morphing scissor structures.

3.2 Case studies for modified scissor units with telescopic rods

3.2.1 Case 6

In this case, the two prescribed target curves are the same as those in Case 1 given in Fig. 2. There are four conventional scissor units and one modified scissor unit (o_3), as shown in Fig. 8a. The end nodes o_1 and o_5 are fixed. The lengths of the straight beams in all conventional scissor units are constrained to remain identical and are denoted as l. The beam lengths in the modified scissor units, denoted as l_1, are also constrained to remain identical. The change of length of the telescopic rods are denoted as g_3^1, g_3^2, g_3^3, g_3^4, and their maximum value with f_3^1, f_3^2, f_3^3, f_3^4 (200 mm). For all scissor units, the relative angles are equal to φ.

Length constraints, relative rotation constraints for the rigid arms, position constraints of all nodes, and boundary constraints can be obtained from Eqs. (3) to (6). However, additional length constraints are formulated to model the change of length of the telescopic rods.

The modified length constraints for the rigid arms at t = 1, 2:

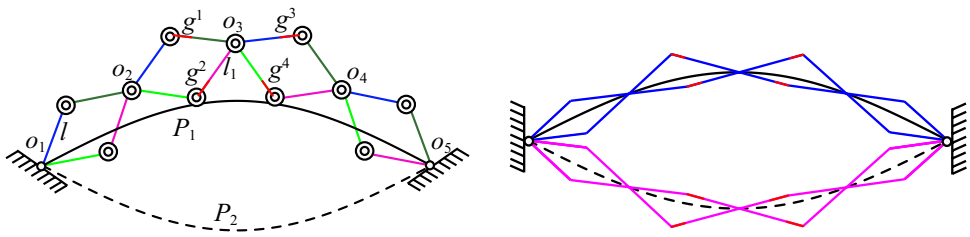

(a) Notations of a scissor unit **(b)** Modified configuration design

Fig. 8 Case 6, modified scissor unit with four telescopic rods

$$
\begin{aligned}
&(x_{o_j^1}^{P_t}-x_{p_j^{1,r}}^{P_t})^2+(y_{o_j^1}^{P_t}-y_{p_j^{1,r}}^{P_t})^2=l^2,(x_{o_j^2}^{P_t}-x_{p_j^{2,r}}^{P_t})^2+(y_{o_j^2}^{P_t}-y_{p_j^{2,r}}^{P_t})^2=l^2,j=1,2,4;\\
&(x_{o_j^1}^{P_t}-x_{p_j^{1,l}}^{P_t})^2+(y_{o_j^1}^{P_t}-y_{p_j^{1,l}}^{P_t})^2=l^2,(x_{o_j^2}^{P_t}-x_{p_j^{2,l}}^{P_t})^2+(y_{o_j^2}^{P_t}-y_{p_j^{2,l}}^{P_t})^2=l^2,j=2,4,5;\\
&(x_{o_j^1}^{P_t}-x_{p_j^{1,l}}^{P_t})^2+(y_{o_j^1}^{P_t}-y_{p_j^{1,l}}^{P_t})^2=(l_1+g_3^{1,P_t})^2,j=3;\\
&(x_{o_j^2}^{P_t}-x_{p_j^{2,l}}^{P_t})^2+(y_{o_j^2}^{P_t}-y_{p_j^{2,l}}^{P_t})^2=(l_1+g_3^{2,P_t})^2,j=3;\\
&(x_{o_j^1}^{P_t}-x_{p_j^{1,r}}^{P_t})^2+(y_{o_j^1}^{P_t}-y_{p_j^{1,r}}^{P_t})^2=(l_1+g_3^{4,P_t})^2,j=3;\\
&(x_{o_j^2}^{P_t}-x_{p_j^{2,r}}^{P_t})^2+(y_{o_j^2}^{P_t}-y_{p_j^{2,r}}^{P_t})^2=(l_1+g_3^{3,P_t})^2,j=3;
\end{aligned}
\tag{8}
$$

Since the telescopic rod can only move in the length direction, there are addition parallel constraints for the node coordinates of the telescopic rods at $t = 1, 2$:

$$
\begin{aligned}
&(x_{s_j^{i,1}}^{P_t}-x_{o_j}^{P_t})(y_{p_j^{1,l}}^{P_t}-y_{s_j^{i,2}}^{P_t})=(x_{p_j^{1,l}}^{P_t}-x_{s_j^{i,2}}^{P_t})(y_{s_j^{i,1}}^{P_t}-y_{o_j}^{P_t}),i=1,2;\\
&\left|y_{s_j^{i,2}}^{P_t}-\frac{(y_{p_j^{1,l}}^{P_t}-y_{s_j^{i,2}}^{P_t})x_{s_j^{i,2}}^{P_t}}{x_{p_j^{1,l}}^{P_t}-x_{s_j^{i,2}}^{P_t}}-\left(y_{s_j^{i,1}}^{P_t}-\frac{(y_{s_j^{i,1}}^{P_t}-y_{o_j}^{P_t})x_{s_j^{i,1}}^{P_t}}{x_{s_j^{i,1}}^{P_t}-x_{o_j}^{P_t}}\right)\right|=0,i=1,2;\\
&(x_{s_j^{i,1}}^{P_t}-x_{o_j}^{P_t})(y_{p_j^{1,r}}^{P_t}-y_{s_j^{i,2}}^{P_t})=(x_{p_j^{1,r}}^{P_t}-x_{s_j^{i,2}}^{P_t})(y_{s_j^{i,1}}^{P_t}-y_{o_j}^{P_t}),i=3,4;\\
&\left|y_{s_j^{i,2}}^{P_t}-\frac{(y_{p_j^{1,r}}^{P_t}-y_{s_j^{i,2}}^{P_t})x_{s_j^{i,2}}^{P_t}}{x_{p_j^{1,r}}^{P_t}-x_{s_j^{i,2}}^{P_t}}-\left(y_{s_j^{i,1}}^{P_t}-\frac{(y_{s_j^{i,1}}^{P_t}-y_{o_j}^{P_t})x_{s_j^{i,1}}^{P_t}}{x_{s_j^{i,1}}^{P_t}-x_{o_j}^{P_t}}\right)\right|=0,i=3,4;
\end{aligned}
\tag{9}
$$

Table 7 gives the optimization results. The optimized configuration is able to morph into the target shapes accurately. The slight asymmetry indicates that other solutions exist.

Table 7 Geometry optimization results in Case 6 for a planar scissor structure with telescopic rods

States	l (mm)	l_1 (mm)	$\varphi(^\circ)$	g_3^1	g_3^2	g_3^2	g_3^4	Configuration error (mm^2)
Initial	519	519	180.00	0	0	0	0	1.63e+13
Curve P_1	420.4	359.73	180.00	142.23	25.63	113.89	2.08	5.59e−11
Curve P_2				26.28	143.01	1.46	113.15	

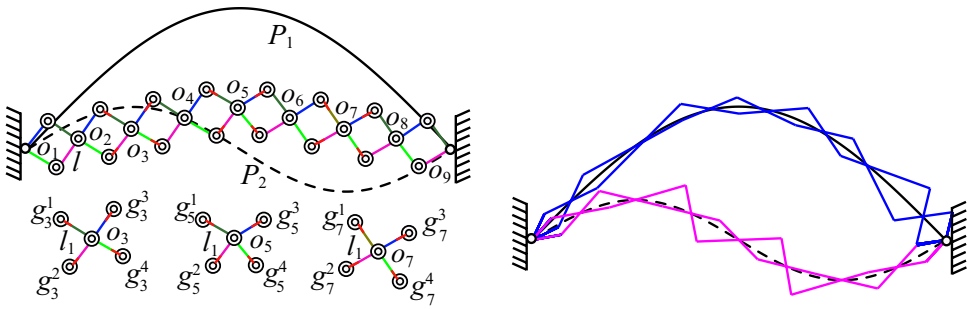

(a) Notations of a scissor unit **(b)** Modified Configuration Design

Fig. 9 Case 7, three modified scissor elements with four telescopic rods

There must be a mirror result. The number of DOFs of the morphing planar scissor structure exceeds the required number to satisfy the two target curves. The modified scissor unit with telescopic rods is more effective in enabling design flexibility compared to adding hinges. The transition between the target shapes is verified as for previous cases that there is a stress-free motion path.

3.2.2 Case 7

More complex target curves are investigated in this section to evaluate the capability enabled by scissor units with telescopic rods. The same target curves in Case 5 are selected, as shown in Fig. 9a. There are six conventional scissor units and three modified scissor units (o_3, o_5 and o_7). The initial geometry and constraint conditions are given. Similar to Case 6, the relative angles are equal to φ, and the lengths of straight beams for all conventional scissor units and modified scissor units are denoted as l and l_1, respectively. For the modified scissor units, the change of length of the telescopic rod and its maximum value are denoted as g_j^i, and f_j^i (set to 300 mm), $i = 1, 2, 3, 4$ and $j = 3, 5, 7$.

Optimization results are shown in Fig. 9b and Table 8. By comparing with Case 5, it can be seen that a better shape fitting is obtained using telescopic rods. The total configuration error of the coordinates reduces by 33.96%, while the average coordinate error increases a little because of the different lengths of straight beams. For the antisymmetric target curve P_2, the optimization problem is non-convex. Moreover, the optimized configuration for the second target curve are asymmetric. There must be an antisymmetric optimization result, indicating a local optimal solution is obtained. The change of length of the telescopic rod enable matching target shapes that feature significant change of curvature. Regarding the degree of freedom, the number of DOFs of the planar scissor structure with three additional hinges in Case 5 is six, while it is twelve for the planar scissor structure with three modified scissor units in Case 7. The latter structure has a larger solution space, it might require a more complex active control system but there is no significant improvement in position accuracy.

3.3 Comparative analysis

Seven cases have been employed to illustrate two strategies for increasing the design flexibility of scissor units, as shown in Table 9. From cases 1, 2 and 3, it can be found that releasing the isometric geometry constraint condition can greatly reduce the coordinate errors without increasing degrees of freedom. Adding modified units is also an effective method to achieve the target configuration, although there are more degrees of freedom, which will increase control complexity. When the target shapes become complex in cases 4 and 5, the shape cannot be controlled within the set error limit (1.0%) by adding hinges. For the scissor structures with telescopic rods, the number of degrees of freedom is higher than that for the corresponding scissor structures with additional hinges. Generally, accurate shape control can be achieved for simple target shapes. If the error limit is relaxed to 10%, both strategies can be employed to morph the structure into the target shapes. This might be appropriate in some cases such for roof structures and arch bridges.

4 Conclusion

The inverse design of morphing planar scissor structures with end constraints has been investigated in this paper. The design process has been formulated into two steps: geometry optimization and motion assessment. In the optimization process based on nonlinear programming, the geometric parameters and the minimization of position deviation of the scissor nodes with respect to target curves are taken as the optimization variables and objective function, respectively. Constrains have been formulated for the length of the straight beams, the relative position of the nodes, the relative rotation of the rigid arms as well as for the boundaries. Five cases have been employed to illustrate the strategy based on adding hinges that allow rotations of rigid arms of the scissor units. Results show that this strategy increases the number of DOFs, and the coordinate error between the predefined and optimized target shapes decreases. A similar conclusion is given for the scissor units equipped with

Table 8 Geometry optimization results in Case 7 for a planar scissor structure with telescopic rods

States	l (mm)	l_1 (mm)	φ(°)	g_3^1	g_3^2	g_3^3	g_3^4	g_5^1	g_5^2
Initial	519	519	180.00	0	0	0	0	0	0
Curve P_1	429	399.97	180.00	222.7	186.1	291.7	199.5	167.4	40.8
Curve P_2				143.6	0	256.8	0	0	211.5
States	g_5^3	g_5^4	g_7^1	g_7^2	g_7^3	g_7^4	Configuration error (mm^2)		
Initial	0	0	0	0	0	0	5.29e+13		
Curve P_1	167.4	40.8	222.7	186.1	291.7	199.5	1.23e+04		
Curve P_2	218.5	0	0	265.6	0	136.2			

Table 9 Comparative analysis for the seven cases with the two strategies

Strategy	Additional hinges					Telescopic rods	
Cases	1	2	3	4	5	6	7
n	5	5	5	9	9	5	9
Number of modified units	1	1	3	3	3	1	3
Length of straight beams	Isometric	Different	Isometric			Isometric	
Target curve f_{P_1}	C_1	C_1	C_1	C_3	C_3	C_1	C_3
Target curve f_{P_2}	C_2	C_2	C_2	C_4	C_5	C_2	C_5
DOF	2	2	6	6	6	4	12
Average coordinate error	13.40%	0	0	1.94%	5.06%	0	6.91%
Optimization result	No	Yes	Yes	No	No	Yes	No

$C_1 = 500\sin(\pi x/3000)$, $C_2 = -500\sin(\pi x/3000)$

$C_3 = 2000\sin(2\pi x/6000)$, $C_4 = 600\sin(\pi|x-3000|/3000)$, $C_5 = 600\sin(2\pi x/6000)$

No: no feasible solution; Yes: feasible solution

telescopic rods. In this case, the change of length of the telescopic rod is effective to enable accurate shape control albeit with a relatively large increase of degrees of freedom.

The influence of target shapes, type of scissor units (conventional scissor units, additional hinges and modified scissor units), constraints of rigid arms are discussed. Releasing the isometric length constraint is a more effective method than increasing the number of modified units. When the number of scissor units is small, optimization results for symmetrical target curves are better than those of asymmetric target curve. The proposed design framework enable morphing between two different target shapes without changing the span length. This proposed method for scissor structures can be used for multifunctional building roofs with various lift environments, arch bridges with different traffic modes and deployable structures. Future work could extend the method proposed in this work to design other types of morphing structures. Besides, future work could look into implementing additional constraints based on practical considerations and coupling the bearing capacity of optimized scissor structures. And more effective objective functions should be investigated to consider the similarity of controlled shapes with target ones to avoid the excessive influence of one shape. Since local optima occurs due to the non-convexity of the problem formulation, a global optimization process could be implemented.

Acknowledgements The work presented in this article was supported by the National Natural Science Foundation of China (Grant Nos. 51822805, 51878147, and U1937202), Postgraduate Research & Practice Innovation Program of Jiangsu Province (SJKY19_0091), Scientific Research Foundation of Graduate School of Southeast University (YBPY2016) and the China Scholarship Council. We would like to thank the anonymous reviewers for their helpful remarks.

Declarations

Conflict of interest The authors declare that they have no conflict of interest.

Replication of results The MATLAB codes of the proposed methods are available upon request to the first and corresponding authors.

References

Akgün Y, Gantes CJ, Kalochairetis KE, Kiper G (2010) A novel concept of convertible roofs with high transformability consisting of planar scissor-hinge structures. Eng Struct 32(9):2873–2883. https://doi.org/10.1016/j.engstruct.2010.05.006

Akgün Y, Gantes CJ, Sobek W, Korkmaz K, Kalochairetis K (2011) A novel adaptive spatial scissor-hinge structural mechanism for convertible roofs. Eng Struct 33(4):1365–1376. https://doi.org/10.1016/j.engstruct.2011.01.014

Alegria Mira L, Thrall AP, De Temmerman N (2014) Deployable scissor arch for transitional shelters. Autom Constr 43:123–131. https://doi.org/10.1016/j.autcon.2014.03.014

Alegria Mira L, Filomeno Coelho R, Thrall A, De Temmerman N (2015) Parametric evaluation of deployable scissor arches. Eng Struct 99:479–491. https://doi.org/10.1016/j.engstruct.2015.05.013

Ario I, Nakazawa M, Tanaka Y, Tanikura I, Ono S (2013) Development of a prototype deployable bridge based on origami skill. Autom Constr 32:104–111. https://doi.org/10.1016/j.autcon.2013.01.012

Arnouts LI, Massart TJ, De Temmerman N, Berke PZ (2019) Computational design of bistable deployable scissor structures: trends and challenges. J Int Assoc Shell Spatial Struct 60:19–34. https://doi.org/10.20898/j.iass.2019.199.031

Arnouts LIW, Massart TJ, De Temmerman N, Berke PZ (2020) Multi-objective optimisation of deployable bistable scissor structures. Autom Constr 114:103154. https://doi.org/10.1016/j.autcon.2020.103154

Bouleau E, Guscetti G (2016) Scissor mechanisms for transformable structures with curved shape. In: Advances in Architectural Geometry, Vdf Hochschulverlag AG an der ETH Zürich

Cai J, Xu Y, Feng J (2013) Kinematic analysis of Hoberman's linkages with the screw theory. Mech Mach Theory 63:28–34. https://doi.org/10.1016/j.mechmachtheory.2013.01.004

Chikahiro Y, Ario I, Nakazawa M, Ono S, Holnicki-Szulc J, Pawlowski P, Graczykowski C, Watson A (2016) Experimental and numerical study of full-scale scissor type bridge. Autom Constr 71:171–180. https://doi.org/10.1016/j.autcon.2016.05.007

Chikahiro Y, Ario I, Pawlowski P, Graczykowski C, Holnicki-Szulc J (2019) Optimization of reinforcement layout of scissor-type bridge using differential evolution algorithm. Comput-Aided Civil Infrastruct Eng 34(6):523–538. https://doi.org/10.1111/mice.12432

Fenci GE, Currie NG (2017) Deployable structures classification: A review. Int J Space Struct 32(2):112–130. https://doi.org/10.1177/0266351117711290

Gantes C (1991) A design methodology for deployable structures, Ph.D. thesis, Massachusetts Institute of Technology

García-Mora CJ, Sánchez-Sánchez J (2020) Geometric method to design bistable and non-bistable deployable structures of straight scissors based on the convergence surface. Mech Mach Theory 146:103720. https://doi.org/10.1016/j.mechmachtheory.2019.103720

García-Mora CJ, Sánchez-Sánchez J (2021) The convergence surface method for the design of deployable scissor structures. Autom Constr 122:103488. https://doi.org/10.1016/j.autcon.2020.103488

Han B, Xu Y, Yao J, Zheng D, Li Y, Zhao Y (2019) Design and analysis of a scissors double-ring truss deployable mechanism for space antennas. Aerosp Sci Technol 93:105357. https://doi.org/10.1016/j.ast.2019.105357

Inoue F, Moroto R, Kurita K, Furuya N (2006) Development of adaptive structure by variable geometry truss (Application of movable monument in EXPO 2005), In: Proceedings of 23th International Symposium on Automation and Robotics in Construction, Tokyo, Japan, pp 704–709

Kaveh A, Abedi M (2019) Analysis and optimal design of scissor-link foldable structures. Eng Comput 35:593–604. https://doi.org/10.1007/s00366-018-0618-2

Kawaguchi K, Sato T, Yang X, Seo N (2019) Development of a deployable geodesic full sphere. J Int Assoc Shell Spatial Struct 60:35–46. https://doi.org/10.20898/j.iass.2019.199.033

Kim T-H, Suh J-E, Han J-H (2021) Deployable truss structure with flat-form storability using scissor-like elements. Mech Mach Theory 159:104252. https://doi.org/10.1016/j.mechmachtheory.2021.104252

Kokawa T, Hokkaido T (1997) Cable scissors arch-marionettic structure: structural morphology, towards the new millennium. In: International Conference of IASS. Nottingham, UK, pp 107–114

Krishnan S, Liao Y (2020) Geometric design of deployable spatial structures made of three-dimensional angulated members. J Architect Eng 26(3):04020029. https://doi.org/10.1061/(ASCE)AE.1943-5568.0000416

Lee D, Popovic Larsen O, Kim S-D (2013) Study of the connection joint for scissor-type deployable structure for the possible application in emergency evacuation shelter. In: Escrig F, Sánchez J (eds) New proposals for transformable architecture, engineering and design, pp 105–109

Li Y, Pellegrino S (2020) A theory for the design of multi-stable morphing structures. J Mech Phys Solids 136:103772. https://doi.org/10.1016/j.jmps.2019.103772

Lim J-S, Choi S-S, Jeong E-S, Kim S-D (2014) An experimental study on the application of shelter structure using deployable scissors systems. J Korean Assoc Spatial Struct 14(3):101–108. https://doi.org/10.9712/KASS.2014.14.3.101

Maden F, Korkmaz K, Akgün Y (2011) A review of planar scissor structural mechanisms: geometric principles and design methods. Architect Sci Rev 54(3):246–257. https://doi.org/10.1080/00038628.2011.590054

Meloni M, Cai J, Zhang Q, Sang-Hoon Lee D, Li M, Ma R, Parashkevov TE, Feng J (2021) Engineering origami: a comprehensive review of recent applications, design methods, and tools. Adv Sci 2000636

Phocas MC, Christoforou EG, Matheou M (2015) Design, motion planning and control of a reconfigurable hybrid structure. Eng Struct 101:376–385. https://doi.org/10.1016/j.engstruct.2015.07.036

Phocas MC, Christoforou EG, Dimitriou P (2020) Kinematics and control approach for deployable and reconfigurable rigid bar linkage structures. Eng Struct 208:110310. https://doi.org/10.1016/j.engstruct.2020.110310

Reksowardojo AP, Senatore G, Smith IF (2019) Experimental testing of a small-scale truss beam that adapts to loads through large shape changes. Front Built Environ 5:93. https://doi.org/10.3389/fbuil.2019.00093

Reksowardojo AP, Senatore G, Smith IF (2020) Design of structures that adapt to loads through large shape changes. J Struct Eng 146(5):04020068. https://doi.org/10.1061/(ASCE)ST.1943-541X.0002604

Rhodes O (2013) Optimal design of morphing structures, Ph.D. thesis, Imperial College London

Roovers K, De Temmerman N (2017) Deployable scissor grids consisting of translational units. Int J Solids Struct 121:45–61. https://doi.org/10.1016/j.ijsolstr.2017.05.015

Sachse R, Bischoff M (2021) A variational formulation for motion design of adaptive compliant structures. Int J Numer Methods Eng 122(4):972–1000. https://doi.org/10.1002/nme.6570

Senatore G, Reksowardojo AP (2020) Force and shape control strategies for minimum energy adaptive structures. Front Built Environ 6:105. https://doi.org/10.3389/fbuil.2020.00105

Senatore G, Duffour P, Winslow P, Wise C (2017) Shape control and whole-life energy assessment of an 'infinitely stiff' prototype adaptive structure. Smart Mater Struct 27(1):015022. https://doi.org/10.1088/1361-665X/aa8cb8

Sleesongsom S, Bureerat S, Tai K (2013) Aircraft morphing wing design by using partial topology optimization. Struct Multidisc Optim 48(6):1109–1128. https://doi.org/10.1007/s00158-013-0944-3

Sun X, Jing X (2016) Analysis and design of a nonlinear stiffness and damping system with a scissor-like structure. Mech Syst Signal Process 66–67:723–742. https://doi.org/10.1016/j.ymssp.2015.05.026

Van Mele T (2008) Scissor-hinged retractable membrane roofs, Ph.D. thesis, Vrije Universiteit Brussel

Wang Y, Senatore G (2020) Minimum energy adaptive structures-all-in-one problem formulation. Comput Struct 236:106266. https://doi.org/10.1016/j.compstruc.2020.106266

Wang Y, Senatore G (2021) Design of adaptive structures through energy minimization: extension to tensegrity. Struct Multidisc Optim 64(3):1079–1110. https://doi.org/10.1007/s00158-021-02899-y

Weaver-Rosen JM, Leal PB, Hartl DJ, Malak RJ (2020) Parametric optimization for morphing structures design: application to morphing wings adapting to changing flight conditions. Struct Multidisc Optim 62(6):2995–3007. https://doi.org/10.1007/s00158-020-02643-y

Yang Y, Peng Y, Pu H, Chen H, Ding X, Chirikjian GS, Lyu S (2019) Deployable parallel lower-mobility manipulators with scissor-like elements. Mech Mach Theory 135:226–250. https://doi.org/10.1016/j.mechmachtheory.2019.01.013

Zhang R, Wang S, Chen X, Ding C, Jiang L, Zhou J, Liu L (2015) Designing planar deployable objects via scissor structures. IEEE Trans Visual Comput Graphics 22(2):1051–1062. https://doi.org/10.1109/TVCG.2015.2430322

Zhang Q, Pan N, Meloni M, Lu D, Cai J, Feng J (2021) Reliability analysis of radially retractable roofs with revolute joint clearances. Reliab Eng Syst Saf 208:107401. https://doi.org/10.1016/j.ress.2020.107401

Zhao J, Chu F, Feng Z (2009) The mechanism theory and application of deployable structures based on SLE. Mech Mach Theory 44(2):324–335. https://doi.org/10.1016/j.mechmachtheory.2008.03.014

Zhao D, Zhao J, Yan Z (2016) Planar deployable linkage and its application in overconstrained lift mechanism. J Mech Robot 8(2):021022. https://doi.org/10.1115/1.4032096